Research Signpost
37/661 (2), Fort P.O., Trivandrum-695 023, Kerala, India

Biomechanics Applied to Computer Assisted Surgery, 2005: 225-241 ISBN: 81-308-0031-4
Editor: Yohan Payan

14

A three-dimensional finite element analysis of stress distribution in a coronary atherosclerotic plaque: *In-vivo* prediction of plaque rupture location

Jacques Ohayon[1], Gérard Finet[2], François Treyve[3], Gilles Rioufol[2] and Olivier Dubreuil[2]

[1]Laboratoire TIMC-IMAG, Equipe DynaCell - CNRS, UMR 5525 - Institut de l'Ingénierie et de l'information de Santé (In^3S) - Faculté de Médecine de Grenoble - 38706 La Tronche cedex France

[2]Department of Hemodynamics and Interventional Cardiology - Hospices Civil de Lyon and Claude Bernard University and CREATIS - Research Unit associated to CNRS (UMR 5515) and affiliated to INSERM - BP Lyon-Monchat - 69394 Lyon Cedex 03 France

[3]Laboratory of Biorheology and Medical Ultrasonics - Research Center – University of Montreal Hospital - Montréal, Québec H2L 2W5, Canada

Abstract

This paper aims at predicting the plaque rupture location of one patient with stable angina and scheduled to undergo percutaneous coronary

Correspondence/Reprint request: Dr. Jacques Ohayon, Laboratoire TIMC-IMAG, Equipe DynaCell - CNRS UMR 5525 - Institut de l'Ingénierie et de l'information de Santé (In^3S) - Faculté de Médecine de Grenoble - 38706 La Tronche cedex France. E-mail: Jacques.Ohayon@imag.fr

intervention. The peak circumferential stress (PCS) is considered as the determining biomechanical factor in the mechanisms leading to rupture of the atherosclerotic plaque and is often used as a predictor of atherosclerotic plaque rupture location. Up to now, to define the site of PCS concentrations, two-dimensional (2D) finite element (FE) analyses were performed on the smallest luminal cross-sectional area of the coronary plaque. In-vivo three-dimensional (3D) FE modeling of atherosclerotic coronaries may be very valuable and more accurate than the 2D FE analysis in helping cardiologists evaluate the risk of spontaneous plaque rupture in a patient. In this work, the performances of the 2D and 3D FE approaches have been compared and the limits of the 2D structural analysis has been pointed out. Our results indicate that the 2D calculations are not always sufficient to define precisely the site of plaque rupture. Not only neglecting biologic factors affecting plaque stability could explain in some cases the poor prediction made with 2D models, but for plaques with complex geometries, the use of a 2D FE approach with a "plane strain" assumption might be also responsible for such low performance. Our 3D model has successfully showed that structural analysis combined with intravascular ultrasound (IVUS) imaging can be used for the in-vivo rupture prediction of complex plaques experimentally triggered by balloon angioplasty.

I. Introduction

Acute coronary syndromes are caused by plaque rupture and, consequently, by an occlusion of the lumen by coronary thrombi. These pathologies comprise unstable angina, non-Q wave myocardial infarction, acute (Q wave) myocardial infarction, and sudden death [1, 2]. Coronary plaques are constantly subject to stress from a variety of mechanical forces, which may exceed the rupture thresholds of the materials going to make them up. The peak circumferential stress (PCS) is considered as the determining biomechanical factor in the mechanisms leading to rupture of the atherosclerotic plaque and is often used as a predictor of atherosclerotic plaque rupture location [3-12].

The characteristics of vulnerable plaque are well defined thanks to several pathological studies [13-15]. Such plaques are characterized by a large lipid pool with a thin fibrous cap [4, 5, 13]. For these atherosclerotic lesions the rupture may occur at any time and cause an acute thrombotic reaction, therefore they are unstable. Previous works have shown that (i) reducing fibrous cap thickness increases the amplitude of the cap peak stress (PCS) exponentially, (ii) the vulnerability to rupture depends on the intrinsic properties of the plaque in question – i.e., the size and consistency of the soft atheromatous core [4], the thickness of the fibrous cap covering the core [4, 15], and inflammation within cap and core [6, 16], and (iii) that the cap stress exceeds the rupture threshold of 300 kPa [3, 17] when the cap thickness becomes lower than 65 μm [4, 15, 18].

Because atherosclerotic plaques are geometrically complex and are composed of different materials [19], biomechanical studies using finite element (FE) methods are performed to investigate the distribution of the stresses and strains on the wall and plaque under physiological loading [3-5, 7-10]. Up to now, the majority of the published finite element (FE) studies on coronary atherosclerotic plaque were based on two-dimensional (2D) geometries of the lesion cross-sections having the smallest luminal area and obtained from histological examination [3, 7, 8, 11, 20], or *ex-vivo* intravascular ultrasound (IVUS) images [9], and more recently from *in-vivo* IVUS images [4, 5]. IVUS is a clinical routine method which gives a qualitative (plaque composition) and quantitative (plaque geometry) analysis of coronary arteries [21]. Since the structural analysis in the previous studies are based on one cross-sectional geometry of the artery, the plaque geometry does not varies with the axial position. However, irregularities along the length of the lesion may affect the stress distribution. In fact, this is an additional reason why the rupture did not always occurs where the peak circumferential stress is located in the plaque [3, 6]. *In-vivo* three-dimensional FE modeling of atherosclerotic coronaries may be very valuable and more accurate than the two-dimensional FE analysis in helping cardiologists evaluate the risk of spontaneous plaque rupture in a patient.

The objectives of this study were: (i) to test, *in-vivo*, the hypothesis that plaque fracture location can be predicted accurately with a three-dimensional (3D) structural analysis using FE method based on IVUS imaging of the coronary lesion, (ii) to compare the spatial stress distributions obtained from the real 3D plaque geometry to those computed from the two-dimensional (2D) modeling of the cross-section having the highest stenosis severity (i.e the smallest luminal area), and (ii) to define and remind the limits of validation of the 2D FE approach. To check the performance of the two computational approaches, we used balloon angioplasty as a plaque rupture trigger. We compared the fracture locations induced by balloon inflation with the high-stress regions predicted from numerical simulations.

II. Methods

This study was performed using computational structural analysis based on typical *in-vivo* intravascular ultrasound (IVUS) images. To compare the *in-vivo* performance between the 2D and 3D FE models, we studied one patient (one man of 50 years) with stable angina and scheduled to undergo percutaneous coronary intervention (PCI) at the Cardiovascular Hospital of Lyon, France. From this patient, arterial geometric configuration of lesion was acquired to initiate FE analysis. The studied lesion was located in the right coronary artery.

This investigation was approved by the institutional board of the Cardiology Department of the Hôpital Cardiologique et Pneumologique of Lyon and the patient was studied only after giving informed consent.

IVUS image acquisition

Lesions were examined by IVUS after the intracoronary administration of 200 μg of nitroglycerine which avoid vasospasms. The IVUS system used was a commercially available mechanical sector scanner (Cardiovascular Imaging Systems, Inc., Sunnyvale, California, USA) with single-element ultrasound catheters (Ultracross 3.5F at 30 MHz and Discovery 2.6F at 40 MHz, Boston Scientific Corp., Watertown, MA, USA). The transducer was advanced more than 10 mm distal to the lesion. The artery was imaged using a motorized pullback at 0.5 mm/s, from the distality of the lesion to the tip of the guiding catheter.

Plaque rupture image acquisition

Balloon angioplasty was used as a plaque rupture trigger in order to check the accuracy of the numerical simulations of plaque rupture location. Balloon inflation was performed until optimal enlargement of the arterial lumen. After balloon deflation, a post-PCI IVUS imaging run was performed, and plaque rupture region was located.

IVUS image analysis

All analyzed images were digitized. Using reproducible landmarks (for example, side branch) and knowing the pullback speed (0.5 mm/s) we precisely determined the same location of pre- and post-PCI lesion cross-sectional images. The cross-section of interest was defined as the smaller pre-PCI lumen cross-section (called lesion cross-section).

Plaque components are characterized by their appearance on IVUS images [22, 23] : i) a highly hypoechogenic component (or anechogenic zone) was suggestive of quasi-cellular tissue (lipid or cellular deposition), ii) a homogeneous reflective component (reflectivity lower or similar than that of the tunica adventitia) was suggestive of organized or disorganized fibrosis, and iii) a hyper-reflective component that heavily attenuates the acoustic signal (a hyper-reflective zone with ultrasound attenuation) was suggestive of calcified plaque. Based on such observations, the contours delimiting lumen border, media, and plaque components (dense fibrosis, cellular fibrosis) were manually traced on each IVUS cross-sectional image obtained before balloon angioplasty. The adventitia contour was added and given a mean 350 μm thickness [24] so as to take account of its protective role against any radial overstretching of the artery [25]. Each of the seventeen obtained pre-PCI cross-sectional image was quantified for lumen cross-sectional area (LA), external elastic membrane cross-sectional area (EEMA), plaque + media cross-sectional area (P + MA = EEMA - LA) and plaque burden (PB =(EEMA -LA)/EEMA) (see Table I).

Table I. Stenosis indexes of each cross-sectional IVUS images. EEMA: external elastic membrane cross-sectional area; PB%: plaque burden in percent (see text for details).

Cross-section number	Luminal area (mm^2)	Plaque + media (mm^2)	EEMA	PB%
1	1122.4	886.7	2009.1	44.1
2	865.0	439.4	1304.3	33.7
3	764.6	1336.0	2100.6	63.6
4	440.8	1893.6	2334.4	81.1
5	359.9	1940.6	2300.5	84.4
6	378.3	2105.6	2483.9	84.8
7	315.2	2388.9	2704.1	88.3
8	262.0	2107.4	2369.4	88.9
9	240.6	1766.6	2007.3	88.0
10	249.6	1725.1	1974.7	87.4
11	245.1	1614.0	1859.1	86.8
12	631.0	1106.0	1737.0	63.7
13	770.8	933.7	1704.4	54.8
14	888.4	765.2	1653.6	46.3
15	951.5	544.6	1496.1	36.4
16	726.6	828.5	1555.1	53.3
17	814.3	611.4	1425.7	42.9

Finite element analysis

Structural computations were performed using the FE method [26]. The FE method is a computerized technique dividing a complex structure into small sections (elements) so that simpler functions may be used to derive the displacement, strain and stress distributions. The obtained 2D plaque contours allow us to simulate the coronary plaque under physiological loading condition. The different plaque constituents and arterial regions were then automatically meshed using ANSYS 8 software (Ansys, Inc., Cannonsburg, PA, USA) on a Personal Computer 2.8GHz. A finite element mesh is composed of small elements, with each element representing a small region of material with a given material law. Moreover knowing that the peak strain may be larger than 20% under physiological pressures [27], finite deformations assumption was required. Notice that in this study, we neglect the residual stresses and we assume that all plaque constituents have a linear elastic behaviors under physiological loading conditions.

Two-dimensional geometries

Finite element analysis are performed individually on each of the seventeen obtained cross-section geometries including the lesion section.

Figure 1 highlights the plaque constituent geometries for three specific cross-sections which are the lesion section (section #9) and its two neighborhood sections #8 and #10. The two cardinal axes East-West and North-South are used as axes of reference. For these computations, the assumption of plane strain was made because the axial dimensions of the plaque are at least the same order of magnitude as its radial dimensions.

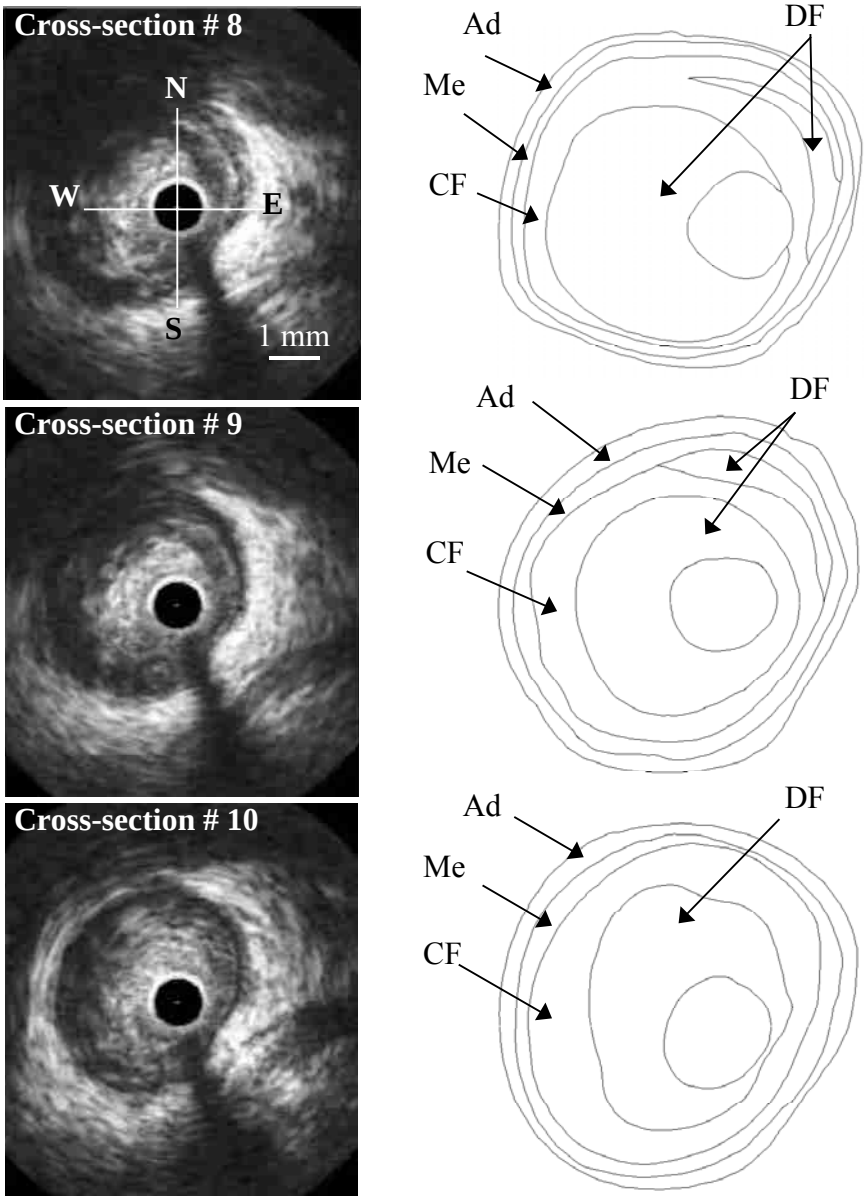

Figure 1. *In-vivo* pre-PCI cross-sectional intravascular ultrasound images number 8, 9 and 10 of the studied plaque. Right column: digitized contours of the three cross-sections. Notice that the cross-section number 9 has the smallest lumen area. Ad: adventitia; Me: media; CF: cellular fibrosis; DF: dense fibrosis; N: north; S: south; E: east; W: west. The dark circle in the middle of the IVUS images represents the catheter of 1 mm of diameter.

The three-dimensional geometry

The 3D plaque geometry of the patient is reconstructed with Ansys software by piling up, all millimeters, seventeen digitized IVUS cross-section images following the trajectory of the center of the catheter. The obtained volume reconstructions of the adventitia, media and lesion constituents are represented in Figs. 2A to 2E. One can note the complex 3D geometries of the

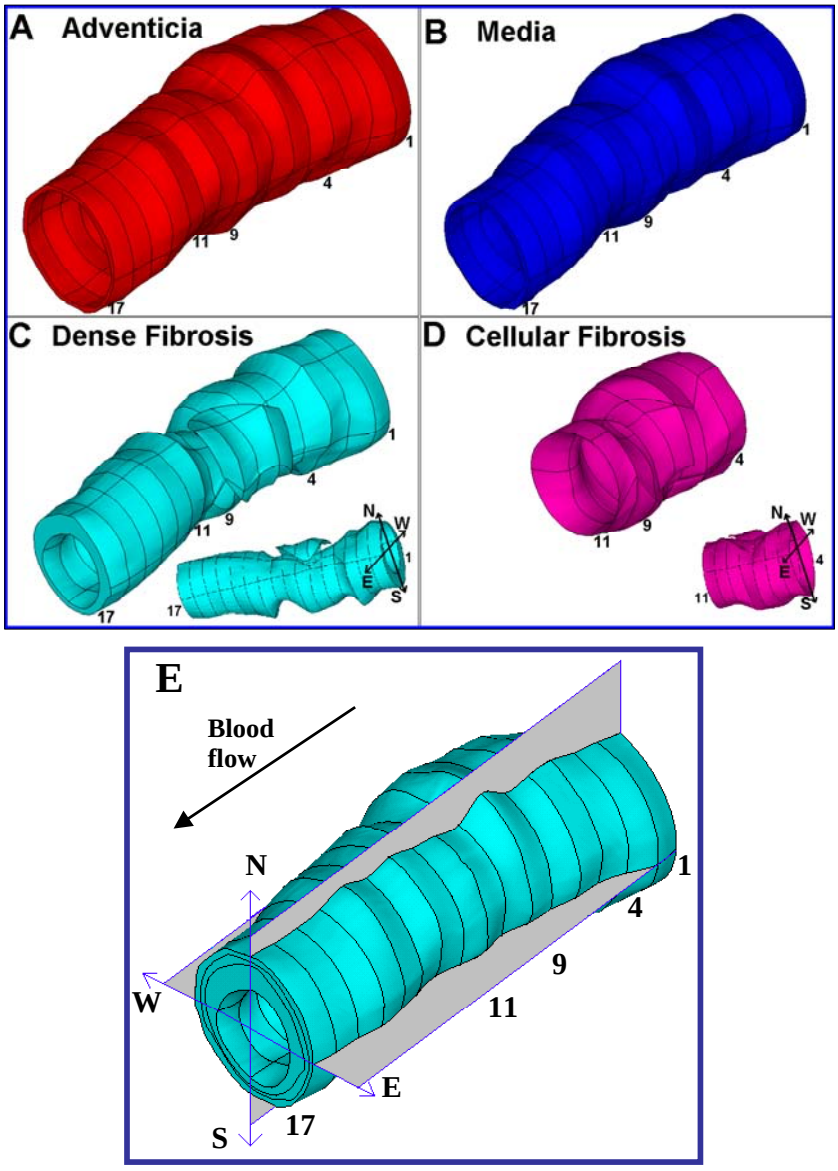

Figure 2. Three-dimensional pre-PCI volume reconstructions of the plaque constituents: **A)** adventicia, **B)** media, **C)** dense fibrosis, **D)** cellular fibrosis and **E)** 3D view of the pathological coronary. The numbers are those of the cross-sections. Inserts in Figs. 2C and 2D represent different views of the same volume geometries. Figure 2E is the final 3D volume reconstruction of the pathological coronary. The sectional work planes defined in Fig. 2E are used to define the boundary conditions (see text for details). N: north; S: south; E: east; W: west.

dense and cellular fibroses volumes (Figs. 2C and 2D) which fit into each other. To compare the peak stress location obtained from the 2D and 3D models, the same two cardinal axes East-West and North-South previously used in the 2D modeling are kept as axes of reference for this 3D reconstruction. The plaque is mainly concentrated between the fourth and the eleventh cross-sections which is the domain where the cellular fibrosis appears (Fig. 2D). In this region the plaque burden PB is larger than 70% (see Table I).

Material properties

To take into account the lamellar structures of the plaques constituents and arterial wall [19], the adventitia, media, dense fibrosis, and cellular fibrosis were modeled as transverse isotropic materials. Thus, the mechanical properties of the deformable mediums were assumed to have the same behavior in the circumferential (θ) and axial (z) directions, and different ones in the radial (r) direction [3]. The full set of rheological parameters using for these all considered materials are given in Table II. Based on the constitutive law found for the healthy wall of the coronary artery and on the assumption that plaque growth induces arterial wall dilation and stretches the wall layers by about 20% [5, 28], we estimate from the uniaxial test the adventitia E_r and E_θ Young's modulus values. The Poisson ratios $\nu_{r\theta}$ and $\nu_{\theta z}$ and other orthotropic material parameters (Young's and shear moduli E_r, E_θ, and $G_{r\theta}$, respectively) for arterial wall and plaque components were those used by Cheng et al. [3]. In agreement with the experimental measurement of Lee et al. [29], it was assumed that the cellular fibrosis characteristics would be slightly more rigid than those of the media. The origin of the r-θ coordinate system for these orthotropic materials was defined as the center of the lumen.

Table II. Material properties used in the finite element analyses for adventitia, media, cellular and dense fibroses. E_r, E_θ and E_z, Young's modulus in the radial (r), circumferential (θ) and axial (z) directions respectively; $\nu_{r\theta}$, ν_{rz} and $\nu_{\theta z}$, Poisson ratios in the r-θ, r-z and θ-z planes respectively; $G_{r\theta}$, G_{rz} and $G_{\theta z}$, shear modulus in the r-θ, r-z and θ-z planes respectively. Most of the data from Loree et al [7] and Finet et al. [4].

	E_r (kPa)	$E_z = E_\theta$ (kPa)	$\nu_{r\theta} = \nu_{rz}$	$\nu_{\theta z}$	$G_{r\theta} = G_{\theta z} = G_{rz}$ (kPa)
Adventicia	80	800	0.01	0.27	400
Media	10	100	0.01	0.27	50
Cellular fibrosis	20	200	0.01	0.27	100
Dense fibrosis	100	1000	0.01	0.27	500

Boundary conditions

Free stress boundary conditions were assumed for the external border of the adventicia, and a physiological mean blood pressure of 13.33 kPa (or 100 mmHg) is applied.

Two-dimensional models

Zero tangential displacement were imposed upon four nodes located at the intersections between the perpendicular work axes (i.e. the two cardinal axes) and the external diameter of the artery. Theses conditions avoid all rigid body translations and rotations.

Three-dimensional model

Again, to avoid all rigid body motion partial displacement limitations are imposed: on the four lines located at the intersections between the two perpendicular work planes and the external surface of the artery, the tangential displacements perpendicular to the luminal axis were set to zero (Fig. 2E). Additionally, the nodes located at the two extremities of the artery are fixed (i.e. zero displacements are imposed on these nodes).

III. Results and discussion

The presented results are focused on the cross-sections having a degree of plaque burden larger than 70% . Thus, the plaque domain of interest is located between the fourth and the eleventh sections (Fig. 2). Moreover the site of the PCS will be given by the amplitude of the angle (in degrees) between the East-West axis and the line going from the center of the lumen to the PCS location. Positive angles are in the North-East region with a zero angle when the PCS is located at the East.

Plaque rupture location

From the post-PCI IVUS images, the ruptured coronary lesion is reconstructed using an 3-D volumetric IVUS software (IôDP, Data Processing, Paris, France) (Fig. 3). It appears that coronary plaque rupture (caused by balloon angioplasty) was detectable from the cross-section #6 to the cross-section #9 with a dissection starting at the cross-section #6 and propagating until cross-section #9.

Two-dimensional simulations

Spatial circumferential stress distributions are computed for each of the seventeen cross-sectional geometries by using individual 2D structural analysis. So, the amplitudes of peak circumferential stresses (PCS) as well as their locations are obtained for each cross-section.

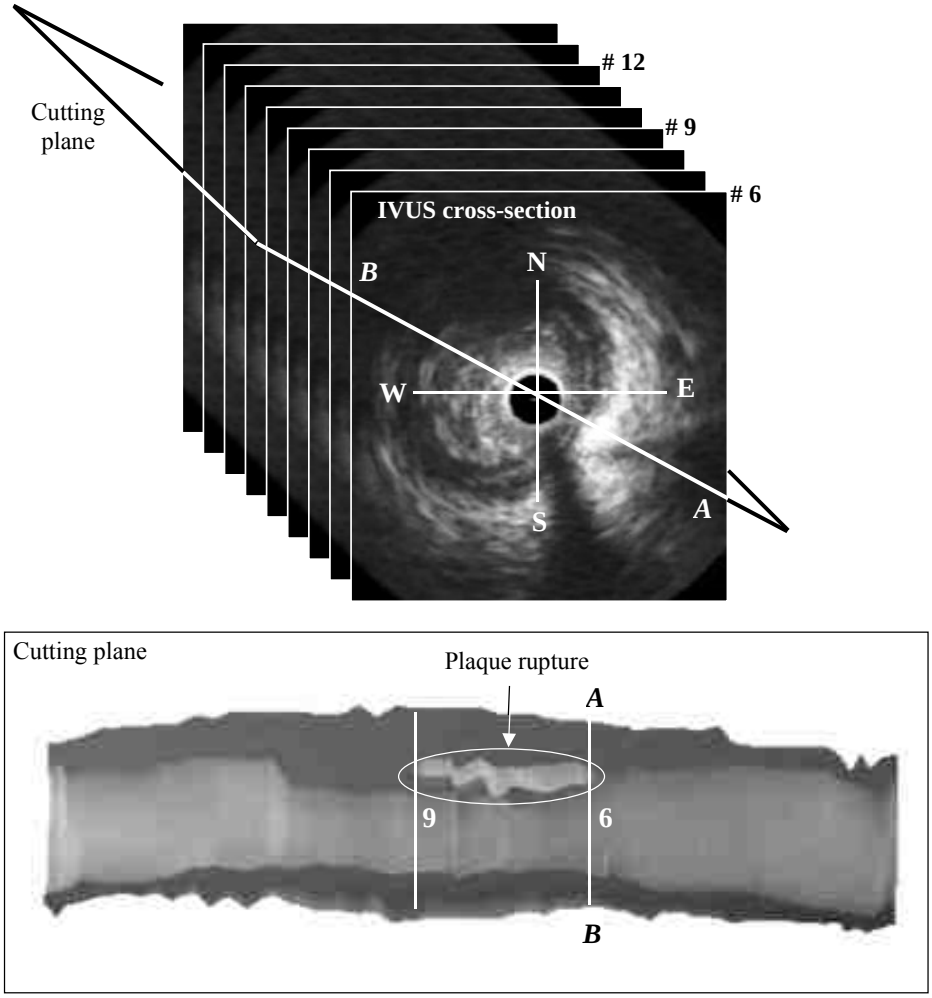

Figure 3. Plaque fracture reconstructed from the post-PCI intravascular ultrasound images. This reconstruction is made on a plane going through the long axis of the artery and of the (AB) line which is defined on the pre-PCI IVUS cross-sectional image #6. The numbers are those of the cross-sections. N: north; S: south; E: east; W: west.

Figure 4 shows that the three considered neighborhood sections have different PCS amplitudes and locations. Interestingly, our results indicate that the higher PCS is not concentrated in the section lesion #9 having the highest stenosis severity (LA = 240.64 mm^2 with a PCS = 78.8 kPa, see Figs. 4, 5A and Table I) but in a proximal section #6 having a lower stenosis severity (LA = 378.28 mm^2 with a PCS = 192.6 kPa, see Fig. 5A and Table I). One can note that even in the close neighborhood of the lesion section #9 the PCS becomes larger than 78.8 kPa (see Fig. 4). Moreover, in the plaque region of interest (i.e. between the cross-sections #4 and #11), the location of the PCS varies between 20° and -70° with a mean value and standard deviation (SD) of -3.9^o ± 42.2. This observed large variability occurs mainly in the close neighborhood of the lesion cross-section #9 (see Figs. 4 and 5B).

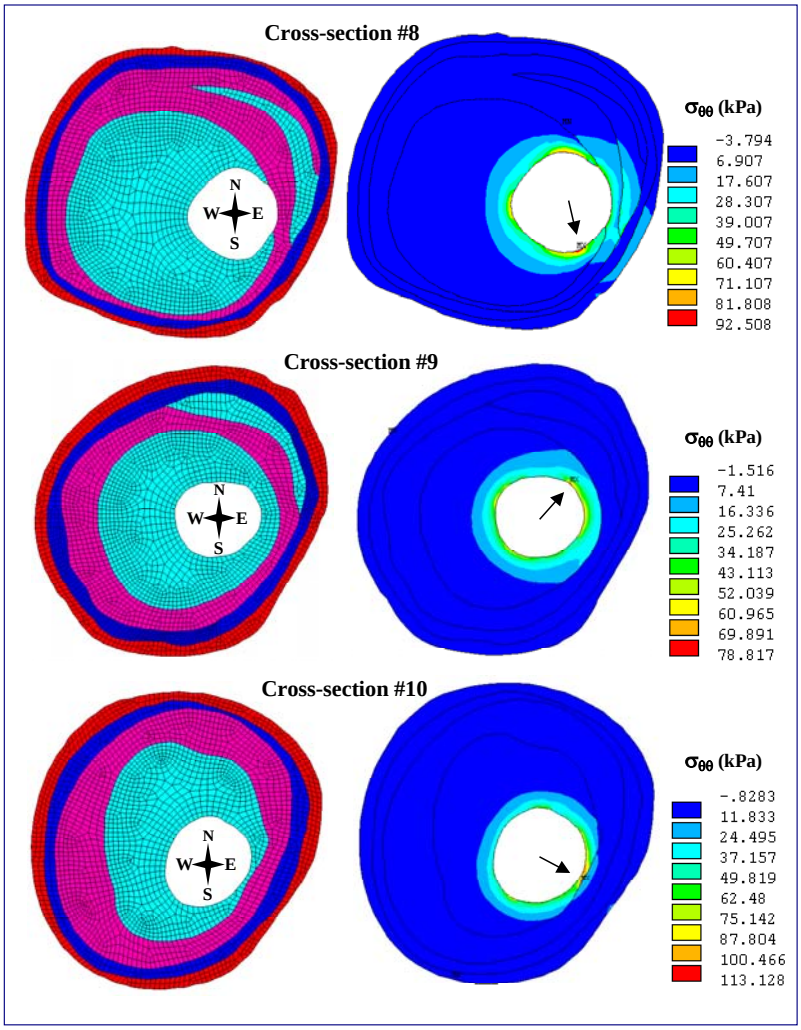

Figure 4. Two dimensional finite element meshes of the three pre-PCI cross-sections number 8, 9 and 10. Red: adventitia; Blue: media; Pink: cellular fibrosis; Turquoise: dense fibrosis; N: north; S: south; E: east; W: west. Right column: circumferential stress maps in kPa. Arrows show peak circumferential stresses (PCSs) for blood pressure levels of 13.33 kPa (100 mmHg).

Three-dimensional simulation

The spatial distribution of the PCS sites derived from the 3D model is quite uniform and the PCSs are located closely on a line parallel to the luminal axis (Fig. 5C). The angular locations of the PCSs vary between -25° and -2° with a mean value and SD of $-5.6^{o}\pm8.8$. Nevertheless, the PCS amplitudes where in the range 33 kPa ≤ PCS ≤ 103 kPa with a mean value and SD of 65.6 kPa±21.4. Interestingly, the line of PCS concentration was found to be located in the region where plaque rupture (dissection) had been visualized during angioplasty (Fig. 3). The maximal PCS is observed at the level of the cross-section # 6 (LA = 378.28 mm^2 with a PCS= 103.5 kPa, see Fig. 5A and Table I) and not on lesion cross-section # 9 (LA = 240.64 mm^2 with a PCS = 69.3 kPa, see Fig. 5A and Table I).

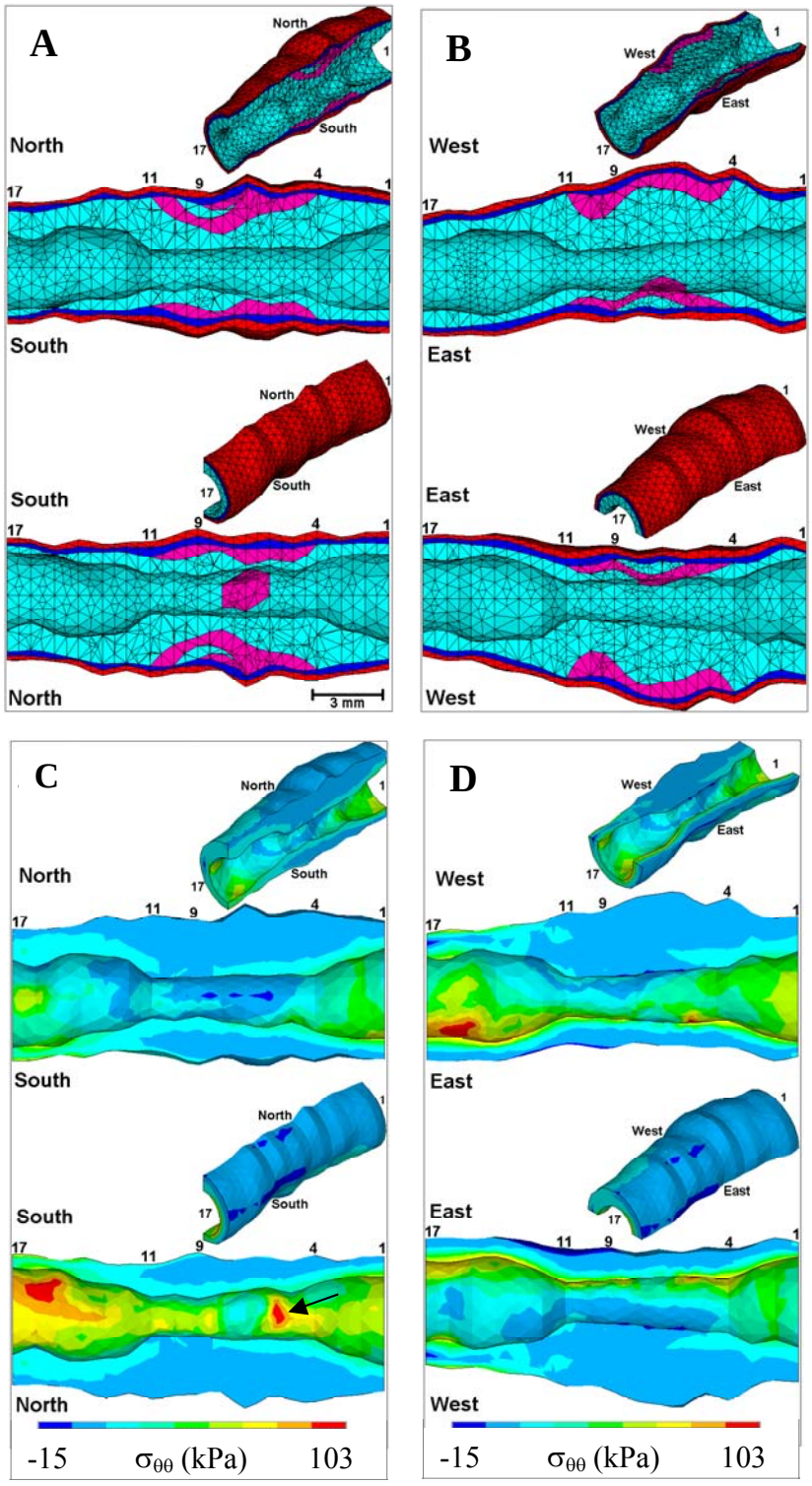

Figure 5. A-B) Three dimensional finite element meshes of the plaque. Red: adventitia; Blue: media; Pink: cellular fibrosis; Turquoise: dense fibrosis. **C-D**) Circumferential stress maps. Arrow on Fig. 5C shows the location where the peak circumferential stress (PCS) for blood pressure level of 13.33 kPa (100 mmHg) is concentrated. $\sigma_{\theta\theta}$: Circumferential stress component.

Notice that other high PCSs occurs in the distal part of the artery (for example section # 16 where LA ≈ 726 and PCS ≈ 103 kPa). But because such cross-sections are not located on the high-stenosis plaque region (i.e. where PB > 70%), we assumed that their morphologies are not responsible for the plaque rupture.

Comparison between two and three-dimensional models

Figures 6A and 6B summarize the results obtained from the performed 2D and 3D simulations. Interestingly and in the light of these results, several remarks can be made:

i) The 2D structural analysis tends to overestimates the amplitude of the PCS (mean value 113.8 kPa ± 44.5 versus 65.6 kPa ± 21.4 for the 3D simulation),
ii) In this plaque, the PCS is not located on the cross-section having the highest stenosis severity (i.e. on section #9).
iii) Compared to the observed pre-PCI plaque rupture, the 3D model predicts quite well the site of PCS concentration (mean angular location $-5.6^{o} \pm 8.8$) which is not the case when considering all 2D individual computations ($-3.9^{o} \pm 42.2$). This last results pointed out the limitation of the plane strain approach for such complex plaque.

Study limitations

Mechanical properties of the plaque constituents

Arterial wall and plaque components exhibit nonlinear mechanical behavior, which can be modeled by hyperelastic constitutive laws [28, 30-34]. The use of a linear elastic behavior causes an under-estimation of the Young's modulus at high values of the loading luminal pressure, and thus may affects the calculation of stresses amplitudes and locations. Nevertheless, the linear approach is considered acceptable for the simulation of arteries under physiological pressure [3-5, 7, 9, 11, 28]. It should also be noted that we are not taken account the pulsatility of the blood pressure which leads to a fatigue phenomena induced by the cyclic loading imposed by blood flow in the arteries. Furthermore, the viscoelastic behavior may be important and must be considered only in more accurate dynamic analysis. Unfortunately, limited data concerning the nonlinear elastic behavior as well as viscoelastic characterization of plaques constituents are available.

Residual stress and unloaded physiological configuration

One of the major limitation when performing computational structural analysis based on *in-vivo* imaging is the determination of the zero stress

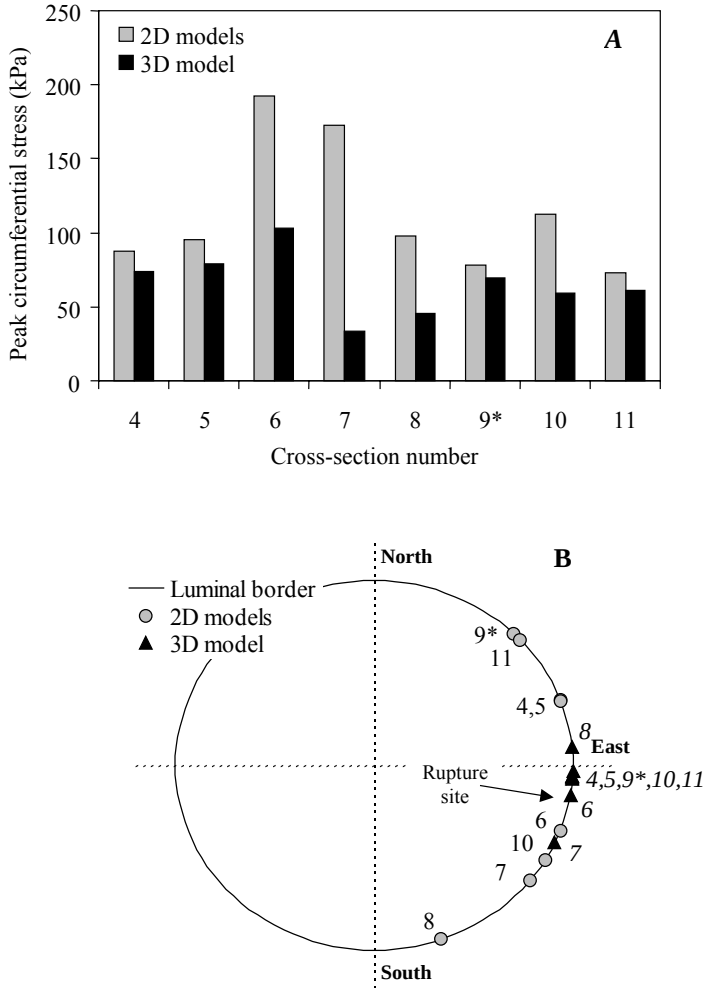

Figure 6. Two and three dimensional peak circumferential stress (PCS) amplitudes and locations obtained from the two finite element (FE) approaches. **A)** Values of the PCS computed in each cross-section using the 2D and the 3D structural FE analyses. **B)** Luminal angular location of the PCS concentrations derived from the 2D and 3D models. The numbers are those of the cross-sections. Asterisk indicates the lesion cross-sectional area with the highest stenosis severity.

configuration of the artery (i.e. free of residual stress). This configuration is needed in order to initiate FE simulations. Obviously, such configuration can not be obtained. Nevertheless, our group was able to approach *in-vivo* the unloaded physiological configuration (i.e. the artery with zero blood pressure) by injection of ATP (Striadyne®, Wyeth Laboratories, Paris, France) which causes a brief atrioventricular block (less than 3 sec) [4, 5]. Unfortunately, this latter configuration could not be known for the studied plaque because the period of the IVUS images acquisition (about 20 sec) was too long compare to the duration of the atrioventricular block. So, neglecting residual stress may modify the PCS amplitude [28, 35, 12].

Clinical implications

Spontaneous rupture of atherosclerotic plaques is known to be involved in the mechanism leading to acute coronary syndromes. Means to detect plaque prone to rupture and to predict rupture location would then be very valuable for clinical diagnosis. In this work our ambition was not to study a full patient population. The aims of the present study were to remind the limits of application for such 2D approaches and to evaluate the performances of structural models using a 2D finite element analysis. To define these limits a complete *in-vivo* reconstruction of plaque has been made in order to perform a realistic three-dimensional structural analysis. This 3D model showed that structural analysis combined with IVUS imaging can be used for the *in-vivo* prediction of plaque rupture location experimentally triggered by balloon angioplasty. Our results indicate that the 2D calculations are not always sufficient to define precisely the site of plaque rupture. Indeed, not only neglecting biologic factors affecting plaque stability could explain the poor prediction of the site of plaque rupture with 2D models, but in some plaques with complex geometries, using a 2D structural model with a "plane strain" assumption might be also responsible for such low performance. It is important to remind that this hypothesis is valid only for long stenosis region but additionally when all cross-sectional plaque morphologies are very similar. Figure 4 shows that this latter condition was not satisfy in our study, therefore a three-dimensional plaque reconstruction from a series of IVUS images needs to be done for realistic structural analysis in the pathologies with complex plaque geometries.

The results of the present study pointed out that in addition to the traditional IVUS image acquisition of the lesion cross-section, several IVUS images must be performed in order to reconstruct the full atherosclerotic plaque before deciding which structural approach must be applied for the plaque rupture location prediction.

The 3D *in-vivo* coronary atherosclerotic plaque model using linear anisotropic constitutive law has been proved to behave in a very realistic way. It is then a reliable tool to test hypothesis about prediction of plaque rupture location. This biomechanical approach of modeling complex plaques will be also used for pathological application as a tool to help cardiologists planning medical gesture during angioplasty or to diagnosis the plaque stability.

Acknowledgement

This work is supported in part by TERUMO France grant. Jacques Ohayon is supported by a grant from the European Community (DISHEART Co-Operative Research Project 2005-2007).

References

1. Falk E, 1989. Morphologic features of unstable atherothrombotic plaques underlying acute coronary syndromes. Am. J. Cardiol., 63 (suppl E):114E-120E.
2. Davies MJ, Thomas AC, 1985. Plaque fissuring: the cause of acute myocardial infarction, sudden ischaemic death, and crescendo angina. Br. Heart J., 53:363-373.
3. Cheng GC, Loree HM, Kamm RD, Fishbein MC, Lee RT, 1993. Distribution of circumferential stress in ruptured and stable atherosclerotic lesions : a structural analysis with histopathological correlation. Circulation, 87 :1179-1187.
4. Finet G., Ohayon J., Rioufol G., 2004. Biomechanical interaction between cap thickness, lipid core composition and blood pressure in vulnerable coronary plaque: impact on stability or instability. Coron Artery Dis., 15:13-20.
5. Ohayon J, Teppaz P, Rioufol G, Finet G, 2001. *In-vivo* prediction of human coronary plaque rupture location using intravascular ultrasound and finite element method. Coron Artery Dis., 12:655-663.
6. Arroyo LH, Lee RT, 1999. Mechanisms of plaque rupture: mechanical and biologic interactions. Cardiovascular Research. 41:369-375.
7. Loree HM, Kamm RD, Stringfellow RG, Lee R, 1992. Effects of fibrous cap thickness on peak circumferential stress in model atherosclerotic vessels. Circ Res., 71:850-858.
8. Huang H, Virmani R, Younis H, et al., 2001. The impact of calcification on the biomechanical stability of atherosclerotic plaques. Circulation, 103:1051-56.
9. Lee RT, Loree HM, Cheng GC, Lieberman EH, Jaramillo N, Schoen FJ, 1993. Computational structural analysis based on intravascular ultrasound imaging before *in vitro* angioplasty : prediction of plaque fracture locations. J Am Coll Cardiol., 21 :777-782.
10. Richardson PD, Davies MJ, Born GVR, 1989. Influence of plaque configuration and stress distribution on fissuring of coronary atherosclerotic plaques. Lancet, 2 :941-944.
11. Veress AI, Cornhill JF, Herdenck EE, Thomas JD, 1998. Age-related development of atherosclerotic plaque stress: a population-based finite element analysis. Coron Artery Dis, 9:13-19.
12. Williamson SD, Lam Y, Youmis HF, Huang H, Patel S, Kaazempur-Mofrad MR, Kamm RD, 2003. On the sen situvity of wall stresses in diseased arteries to variable material properties. Journal of Biomedical Engineering, 125:147-155.
13. Davies MJ, 1996. Stability and instability : two faces of coronary atherosclerosis. Circulation, 94:2013-20.
14. Falk E, Shah PK, Fuster V, 1995. Coronary plaque disruption. Circulation, 92:657-71.
15. Virmani R, Kolodgie FD, Burke AP, et al., 2000. Lesions from sudden coronary death : a comprehensive morphological classification scheme for atherosclerotic lesions. Arterioscler Thromb Vasc Bio, 20 :1262-75.
16. Lee RT, 2000. Atherosclerotic lesion mechanics versus biology. Z. Kardiol., 89:80-84.
17. Lendon CL, Davies MJ, Born GV, Richardson PD, 1991. Atherosclerotic plaque caps are locally weakened when macrophage density increased. Atherosclerosis, 87:87-90.

18. Moreno PR, Purushothaman R, Fuster V, O'Connor WN, 2002. Intimomedial interface damage and adventitial inflammation is increased beneath disrupted atherosclerosis in the aorta: implications for plaque vulnerability. Circulation, 105:2504-2511.
19. Clark JM, Glagov S, 1985. Transmural organisation of the arterial media: the lamellar unit revisited. Arteriosclerosis, 5 :19-34.
20. Beattie D, Xu C, Vito R, Glagov S, Whang MC, 1998. Mechanical analysis of heterogeneous, atherosclerotic human aorta. J. Biomech Eng., 120:602-607.
21. Bocksch W, Schartl M, Beckmann S, Dreysse S, Fleck E, 1997. Intravascular ultrasound assessment of direct percutaneous transluminal coronary angioplasty in patients with acute myocardial infarction. Coron. Arte. Dis., 8:265-273.
22. Palmer ND, Northridge D, Lessells A, McDicken WN, Fox KAA, 1999. In vitro analysis of coronary atheromatous lesions by intravascular ultrasound. Eur. Heart J., 20:1701-6.
23. Di Mario C, Gorge G, Peters R, et al., 1998 Clinical applications and image interpretation in intracoronary ultrasound. Eur. Heart J., 19:207-229.
24. Rioufol G, Finet G, Tabib A, et al., 1999. The (often) four-layer apparence of coronary arteries by intravascular ultrasound: the tunica adventitia. J Am Coll Cardiol., 16(abstract) :77A.
25. Rachev A, 1997. Theoritical study of the stress-dependent remodeling on arterial geometry under hypertensive conditions. J Biomechanics, 30 :819-827.
26. Bathe KJ, 1982. Finite Element Procedures in Engineering Analysis. Ed. Prentice-Hall, Inc., Englewood Cliffs, New Jersey.
27. Tajaddini A, Kilpatrick D, Vince DG, 2003. A novel experimental method to estimate stress-strain behavior of intact coronary arteries using intravascular ultrasound (IVUS). ASME J Biomech Eng., 125:120-123.
28. Teppaz P., Finet G., Tabib A., Rioufol G., Ohayon J., 1999. Evaluation des contraintes résiduelles dans les artères coronaires humaines normales. Innov. Techn. Biol. Med., 20(1):59-66.
29. Lee RT, Grodzinsky AJ, Frank EH, Kamm RD, Schoen FJ, 1991. Structure-dependent dynamic mechanical behavior of fibrous caps from human atherosclerotic plaques. Circulation, 83:1764-1770.
30. Oh S, Kleinberger M, McElhaney JH, 1994. Finite element analysis of balloon angioplasty. Med Biol Eng Comput., 32:S108-S114.
31. Holzapfel GA, Weizsäcker HW, 1998. Biomechanical behavior of the arterial wall and ist numerical characterization. Comput Med Biol., 28:377-392.
32. Schulze-Bauer CAJ, Holzapfel GA, 2003. Determination of constitutive equations for human arteries from clinical data. J. Biomechanics, 36:165-169.
33. Lally C, Reid AJ, Prendergast PJ. 2004. Elastic behavior of porcine coronary artery tissue under uniaxial and equibiaxial tension. Annals of Biomedical Engineering, 32(10):1355-1364.
34. Holzapfel GA, 2000. Non linear solid mechanics. John Wiley and sons, Ltd
35. Matsumoto T, Hayashi K, Ide K, 1995. Residual stain and local strain distributions in the rabbit atherosclerotic aorta. J. Biomechanics, 28(10):1207-1217